

Multi-objective Parameter Optimization of Common Land Model Using Adaptive Surrogate Modelling

Wei Gong¹, Qingyun Duan¹, Jianduo Li¹, Chen Wang¹, Zhenhua Di¹, Yongjiu Dai¹,
Aizhong Ye¹, Chiyuan Miao¹

¹College of Global Change and Earth System Science (GCESS), Beijing Normal University, Beijing, 100875, and Joint Center for Global Change Studies, Beijing, 100875, China

(gongwei2012@bnu.edu.cn, qyduan@bnu.edu.cn, lijian duo@mail.bnu.edu.cn,
wangchen@mail.bnu.edu.cn, zhdi@bnu.edu.cn, yongjiudai@bnu.edu.cn, azye@bnu.edu.cn,
miaocy@vip.sina.com)

Abstract:

Parameter specification usually has significant influence on the performance of land surface models (LSMs). However, estimating the parameters properly is a challenging task due to the following reasons: (1) LSMs usually have too many adjustable parameters (20 to 100 or even more), leading to the curse of dimensionality in the parameter input space; (2) LSMs usually have many output variables involving water/energy/carbon cycles, so that calibrating LSMs is actually a multi-objective optimization problem; (3) Regional LSMs are expensive to run, while conventional multi-objective optimization methods need a large number of model runs (typically $10^5\sim 10^6$). It makes parameter optimization computationally prohibitive. An uncertainty quantification framework was developed to meet the aforementioned challenges, which include the following steps: (1) using parameter screening to reduce the number of adjustable parameters; (2) using surrogate models to emulate the responses of dynamic models to the variation of adjustable parameters; (3) using an adaptive strategy to improve the efficiency of surrogate modeling based optimization; (4) using a weighting

30 function to transfer multi-objective optimization to single objective optimization. In
31 this study, we demonstrate the uncertainty quantification framework on a single column
32 application of a land surface model – the Common Land Model (CoLM) and evaluate
33 the effectiveness and efficiency of the proposed framework. The result indicate that
34 this framework can efficiently achieve optimal parameters in a more effective way.
35 Moreover, this result implies the possibility of calibrating other large complex dynamic
36 models, such as regional-scale land surface models, atmospheric models and climate
37 models.

38

39 **Keywords:**

40 Land surface model; multi-objective optimization; parameter calibration; surrogate
41 modeling; statistical emulator; adaptive sampling;

42

43 **1. Introduction**

44 Land surface models (LSMs), which offer land surface boundary condition for
45 atmospheric models and climate models, are widely used in weather and climate
46 forecasting. They are also a tool for studying the impacts of climate change and human
47 activities on our environment. Parameters of land surface models usually have
48 significant influence on their simulation and forecasting capability. It has been shown
49 that tuning even one or two parameters may significantly enhance the simulation ability
50 of a land surface model (e.g., [*Henderson-Sellers et al.*, 1996; *Liang et al.*, 1998;
51 *Lohmann et al.*, 1998; *Wood et al.*, 1998]). How to specify the parameters in a LSM
52 model properly, however, remains a very challenging task because the LSM parameters
53 are usually not directly measurable at the scale of model applications.

54 Automatic optimization approaches have been frequently used in calibrating the
55 parameters of hydrological models. There is a plethora of optimization approaches
56 available, including single-objective optimization methods such as SCE-UA [*Duan et*
57 *al.*, 1992; *Duan et al.*, 1993; *Duan et al.*, 1994], SCEM-UA [*Vrugt et al.*, 2003], genetic
58 algorithm [*Wang*, 1991], and multi-objective optimization methods such as MOCOM-
59 UA [*Boyle et al.*, 2000; *Boyle*, 2000; *Gupta et al.*, 1998; *Yapo et al.*, 1998] and

60 MOSCEM-UA[Vrugt *et al.*, 2003].

61 Compared to traditional hydrological models, the parameter calibration approach
62 has not been practiced as much in LSM community, especially for large spatial scale
63 applications. The major obstacles to calibrating land surface models over a large spatial
64 scale are: (1) there are too many parameters to calibrate, (namely, the curse of
65 dimensionality in parameters); (2) dimensionality of the output space is too high (i.e.,
66 many processes such as water/energy/carbon cycles are simulated simultaneously); (3)
67 conventional optimization methods, especially multi-objective approach, need a large
68 number ($\sim 10^5$ - 10^6) of model runs; and the large complex dynamic system models such
69 LSMs are usually expensive to run (i.e., costing many CPU hours). There have been
70 numerous attempts to use multi-objective optimization to calibrate the parameters of
71 land surface models and significant improvement in LSM performance measures as a
72 result of optimization have been reported (e.g., [Bastidas *et al.*, 1999; Gupta *et al.*, 1999;
73 Leplastrier *et al.*, 2002; Xia *et al.*, 2002]). However, the optimization efforts in the past
74 were usually limited to cases studies involving only point or limited spatial domain-
75 scale applications of LSMs [Liu *et al.*, 2003; Liu *et al.*, 2004; 2005]. To take a multi-
76 objective optimization approach to the calibration of LSM parameters for large scale
77 applications, the key is to reduce the number of model runs to an appropriate level that
78 we can afford.

79 Surrogate based optimization is one of the most commonly used approaches to
80 optimizing large complex dynamic models. Several books and literature reviews have
81 described the advances of surrogate based optimization in recent years [e.g., Jones,
82 2001; Ong *et al.*, 2005; Jin, 2011; Koziel and Leifsson, 2013; and Wang *et al.*, 2014].
83 Surrogate based optimization has been applied to economics, robotics, chemistry,
84 physics, civil and environmental engineering, computational fluid dynamics, aerospace
85 designs, et al [Gorissen, 2010]. On the development of surrogate based optimization,
86 Jones *et al.* [1998] proposed EGO (Effective Global Optimizer) for expensive models
87 using ‘DACE stochastic process model’, namely Kriging interpolation method, as
88 surrogate model. Castelletti *et al.* [2010] developed a multi-objective optimization
89 method for water quality management using radial basis function, inverse distance

90 weighted and n-dimensional linear interpolator as surrogates. Loshchilov et al. [2010]
91 investigated the use of ranked-based Support Vector Machine and demonstrated that for
92 surrogate based optimization capturing the relative value of the objective functions is
93 more important than reducing the absolute fitting error. Pil  and Neruda [2013]
94 developed a surrogate model selector for multi-objective surrogate-assisted
95 optimization. In hydrology and water resources, Razavi et al. [2012] has summarized
96 recent applications, advantages, and existing problems. Wang et al. [2014] evaluated
97 the influence of initial sampling and adaptive sampling methods for surrogate-assisted
98 optimization of a simple hydrological model, SAC-SMA model. Song et al. [2012]
99 optimized the parameter of a distributed hydrological model-DTVGM model's
100 parameter with SCE-UA algorithm using MARS method [Friedman, 1991] as surrogate.

101 In our recent works, we proposed a framework that can potentially reduce the
102 number of model runs needed for parameter calibration of large complex system models
103 [Wang et al., 2014]. This framework involves the following steps: (1) a parameter
104 screening step using global sensitivity analysis to identify the most sensitive parameters
105 to be included in the optimization; (2) surrogate modelling that can emulate the
106 response surface of the dynamic system model to the change in parameter values; (3)
107 an adaptive sampling strategy to improve the efficiency of the surrogate model
108 construction; (4) a multi-objective optimization step to optimize the most sensitive
109 parameters of the dynamic system model. In this paper, we will illustrate this parametric
110 uncertainty quantification framework with the Common Land Model (CoLM), a widely
111 used, physically based land surface model developed by Yongjiu Dai and colleagues
112 [Dai et al., 2003; Dai et al., 2004; Ji and Dai, 2010]. The work related to parameter
113 screening and surrogate modeling based optimization (ASMO) method for single
114 objective has already been published [Li et al., 2013; Wang et al., 2014]. This paper
115 will emphasize on the analysis of different surrogate model construction methods and
116 multi-objective optimization method and results.

117 This paper contains the following parts: section 2 introduces the basic information
118 of CoLM, the study area and dataset, the adjustable parameters and the output variables
119 to be analyzed; section 3 presents an inter-comparison of 5 surrogate modeling methods,

120 and discusses how many model runs would be sufficient to build a surrogate model for
 121 optimization; section 4 carries out single and multiple objective optimization using an
 122 adaptive surrogate model based optimization strategy (ASMO); section 5 provides the
 123 discussion and conclusions.

124

125 **2. Experiment setup**

126 **Model and Parameters**

127 Common Land Model (CoLM) proposed by Yongjiu Dai and colleagues [*Dai et al.*,
 128 2003; *Dai et al.*, 2004; *Ji and Dai*, 2010] is one of the most widely used land surface
 129 model in the world. It combines the advantages of Land Surface Model (LSM) [*Bonan*,
 130 1996], Biosphere-atmosphere transfer scheme (BATS) [*Dickinson et al.*, 1993] and
 131 Institute of Atmospheric Physics land-surface model (IAP94) [*Dai and Zeng*, 1997; *Dai*
 132 *et al.*, 1998]. CoLM considers physical processes of energy and water transmission in
 133 soil vegetation, snow cover and atmosphere. It also implements glacier, lake, wetland
 134 and dynamic vegetation processes. Similar to previous research in presented in [*Li et*
 135 *al.*, 2013], we select 40 adjustable parameters from CoLM. The parameter names,
 136 physical meanings and value ranges are shown in **Table 1**.

137

[Table 1]

138 This study considers six output variables simulated by CoLM: sensible heat, latent
 139 heat, upward longwave radiation, net radiation, soil temperature and soil moisture. The
 140 Normalized Root Mean Squared Error is used as the objective function in our analysis:

$$NRMSE_i = \frac{\sqrt{\sum_{j=1}^N (y_{i,j}^{sim} - y_{i,j}^{obs})^2}}{\sum_{j=1}^N y_{i,j}^{obs}} \quad (1)$$

141 where i is the index of output variables, j is the index of time step, N is the total number
 142 of observations, $y_{i,j}^{sim}$ and $y_{i,j}^{obs}$ are the simulated and observed values, respectively.
 143 Objective functions represent the performance of model simulation and a smaller
 144 objective function means better performance.

145

146 **Study area and datasets**

147 The study area and associated datasets are from the Heihe river basin, the same as
148 in [Li et al., 2013]. The Heihe river basin, which is located between 96 °42'-102 °00'E
149 and 37 °41'-42 °42'N, is an inland river basin in the arid region of northwest China. The
150 basin area is approximately 130,000 km² and its altitude varies from sea level to 5500m.
151 The Heihe river basin has a variety of land using types including forest, grassland,
152 farmland, and glacier, among others, making it an ideal research region for LSM
153 simulation. In this research we use the data from A'rou observation station located at
154 the upstream region of the Heihe river basin. Its geographic coordinate is 100 °28'E,
155 38 °03'N, altitude is 3032.8m above sea level and the land cover type is alpine steppe.

156 The forcing data used include downward shortwave and longwave radiation,
157 precipitation, air temperature, relative humidity, air pressure and wind speed [Hu et al.,
158 2003]; and the observation data used to validate the simulation of CoLM include:
159 sensible heat, latent heat, upward longwave radiation, net radiation, soil temperature
160 and soil moisture. The soil temperature and moisture were measured at depth 10cm,
161 20cm, 40cm and 80cm. In CoLM, the soil is divided into 10 layers and the simulated
162 soil temperature and soil moisture are linearly interpolated to the measured depth.
163 Currently we have 2 years observation data. The data from year 2008 was used for spin
164 up and that of 2009 was used for parameter screening, surrogate modeling and
165 optimization. The simulation time step is set to 30 minutes and the simulation outputs
166 are averaged to 3 hours in order to compare with the observation data.

167

168 **3. Comparison of Surrogate models**

169 After the sensitive parameters are identified using global sensitivity methods (see
170 [Li et al., 2013]), the next step is to calibrate the sensitive parameters through multi-
171 objective optimization. Since the calibration of CoLM in real world applications can be
172 very expensive, we aim to establish a surrogate model to represent the response surface
173 of the dynamic CoLM. Surrogate model, also called response surface, meta-model,
174 statistical emulator, is a statistical model that describes the response of output variable
175 to the variation of input variables. Because the surrogate model only considers the
176 statistical relationship between input and output, it is usually much cheaper to run than

177 the original large complex dynamic model (“original model” for short). Parameter
 178 optimization usually needs thousands, or even up to millions times of model runs. It
 179 will be impossible to calibrate large complex dynamic models if running the original
 180 dynamic model is too time consuming. If we can do parameter optimization with
 181 surrogate model instead of original model, the time of running original model will be
 182 dramatically reduced, making it possible to calibrate the large complex dynamic models,
 183 such as land surface models, atmospheric models, or even global climate models.
 184 However, optimization based on surrogate models can be a challenging task because
 185 the response surface might be very bumpy and has many local optima. *Razavi et al.*
 186 [2012] gave a comprehensive review of the surrogate modeling methods and
 187 applications in water resources, and discussed the pitfalls of surrogate modeling as well.

188 In this research, we first compared 5 different surrogate models: Multivariate
 189 Adaptive Regression Spline (MARS), Gaussian Process Regression (GPR), Random
 190 Forest (RF), Support Vector Machine (SVM), and Artificial Neural Network (ANN). A
 191 brief introduction of these methods is provided in the **Appendix**. To build a surrogate,
 192 we need to choose a sampling method first. The sampling method used in this study is
 193 Latin Hypercube Sampling (LH) [*McKay et al.*, 1979]. The sample sizes are set to 50,
 194 100, 200, 400, 800, 1200, and 2000, respectively. The inter-comparison results are
 195 shown in **Figure 1** and **Figure 2**, in which the x-axis is the sample size, and y-axis is
 196 the NRMSE (i.e., the ratio of the root mean square error (RMSE) of the simulation
 197 model and the surrogate model). **Figure 1** shows the error of the training set, namely
 198 the NRMSE between the outputs predicted by the surrogate model and the outputs of
 199 the training samples, and **figure 2** shows the NRMSE of the testing set. Since every
 200 sample set of each size was independently generated, we use the 2000 points set to test
 201 50, 100, 200, 400, 800 and 1200 points set, and use the 1200 one to test the 2000 one.
 202 For each output variable, we only construct surrogate models for the most sensitive
 203 parameters based on the screening results obtained by *Li* [2012] and *Li et al.* [2013]
 204 (see **Table 2**).

205 **[Table 2]**

206 As shown in **Figure 1**, for some cases, such as upward longwave radiation, the

207 fitting ability of the training set does not change significantly with sample size, but for
208 soil moisture, larger sample size leads to better fitted surrogate models. Such
209 phenomenon indicated that the specific features of the response surfaces have
210 significant influence on the fitting ability, and good surrogate models must have the
211 ability to adapt to those features. As shown in **Figure 1**, GPR has the best fitting ability
212 for almost every case except soil temperature. As described in Appendix 2, the hyper-
213 parameters used by GPR can be adaptively determined using the maximum marginal
214 likelihood method.

215 **Figure 2** shows the NRMSE of the testing sets, indicating the risk of over-fitting.
216 In Figure 2 we can note more remarkable findings: (1) The error of a surrogate model
217 decreases as the sample size increases. The marginal benefits of using additional
218 samples become less or even negligible if the sample size is larger than 400; (2) Among
219 the 5 different surrogate models, GPR has the best performance, while ANN ranks the
220 second. RF and MARS have lower accuracy. For some output variables (e.g., sensible
221 and latent heat), the performance of SVM seems acceptable, while for other variables
222 (e.g., soil temperature), SVM's performance is not satisfactory; (3) The convergence
223 speeds for the 6 output variables are different. For net radiation, soil temperature and
224 soil moisture, the fitting error decreases to nearly zero if the sampling points are more
225 than 200; while for sensible heat, latent heat and upward long-wave radiation, the
226 marginal benefit of adding more points is still significant beyond more than 200 sample
227 points. Since the GPR method can consistently give the best performance for all the 6
228 output variables, we choose GPR in the multi-objective optimization analysis presented
229 later.

230 [Figure 1]

231 [Figure 2]

232

233 4. Optimization

234 4.1 Single-objective optimization

235 Before we conduct multi-objective optimization, we first carried out single-
236 objective optimization for each output variable using the GPR surrogate model. The

237 Shuffled Complex Evolution (SCE) method [Duan *et al.*, 1992; Duan *et al.*, 1993; Duan
 238 *et al.*, 1994] is used to find the optima of the surrogate models. In order to figure out
 239 how many sample points are sufficient to construct a surrogate model for optimization,
 240 different sample sizes (i.e., 50, 100, 200, 400, 800, 1200, and 2000) are experimented.
 241 To evaluate the optimization results based on the surrogate model, we also set up two
 242 control cases: (1) No optimization using the default parameters as specified in CoLM.
 243 (2) Optimization using the original CoLM (i.e., no surrogate model is used). The second
 244 case is referred as “direct optimization”. The control cases are used to confirm the
 245 following hypotheses: (1) Parameter optimization can indeed enhance the performance
 246 of CoLM. (2) Optimization using the surrogate model can achieve similar optimization
 247 result as using the original model, but with fewer model runs.

248 The optimal parameters given by single-objective optimization are shown in
 249 **Figure 3**. In each subfigure the optimal parameter values are normalized to [0, 1]. The
 250 bold black line is the optimal parameter set obtained by direct optimization using the
 251 original CoLM, and other lines are optimal parameters given by surrogate models
 252 created with different sample sizes. **Table 3** summarizes the optimized NRMSE values
 253 of all surrogate model based optimization runs with different sample sizes, as well as
 254 the control cases. The numbers of original model runs that SCE takes are also listed in
 255 the brackets.

256

257 [Figure 3]

258 [Table 3]

259

260 The optimization results reveal that: (1) Parameter optimization can significantly
 261 improve the simulation ability of CoLM for all output variables; (2) For sensible heat,
 262 upward longwave radiation, net radiation, soil moisture, the optimal parameters
 263 obtained by surrogate model optimization runs are very similar to those obtained by
 264 direct optimization. The optimal parameters obtained for different sample sizes are also
 265 close to each other. For latent heat and soil temperature, however, the optimal
 266 parameters given by surrogate model optimization and direct optimization are

267 significantly different. The discrepancy between the results with different sample sizes
268 is also significant, comparing to the previous 4 outputs; (3) Surprisingly, for four of the
269 outputs, namely some variables (e.g., sensible heat, upward longwave radiation, net
270 radiation and soil moisture), sample size does not have significant influence on the
271 optimization results. As shown in **table 3**, even a surrogate model constructed with 50
272 samples is similar to the one constructed with 2000 samples and with the direct
273 optimization. For soil temperature, 200 samples are sufficient, and for latent heat, more
274 than 400 samples are enough. Interestingly, the LH50's optimization result for sensible
275 heat is even smaller than that of LH2000. This is because LH sampling is random and
276 the LH 50 sampling may have produced a sample point very close to the global
277 optimum, while the best sample point of LH2000 sampling may be further away from
278 the global optimum. Consequently, the number of samples required for surrogate based
279 optimization varies for different outputs because of the randomness of sampling designs,
280 and the complexity of response surfaces. A more complex surface needs more sample
281 points to build an effective surrogate model, compared to simple surface. Even so, this
282 result is very encouraging that with the help of surrogate models we can possibly reduce
283 the number of model runs required by optimization down to hundreds of times; (4) The
284 number of original model runs that SCE takes before convergence is also listed in **Table**
285 **3**. The result indicated that SCE can get better, or similar optimal NRMSE, but the
286 number of model runs is larger than that using surrogate model. If the original dynamic
287 model costs too much CPU time to run, surrogate based optimization can be more
288 efficient than the SCE; (5) Different output variables require different optimal
289 parameters, indicating the necessity of multi-objective optimization. For example, P6,
290 the Clapp and Hornberger "b" parameter, is sensitive to many outputs. For sensible heat,
291 latent heat and soil moisture, the optimal value of P6 is high, while for upward
292 longwave radiation, net radiation and soil temperature, the optimal value of P6 is low.
293 In order to balance the performance of all output variables, it is necessary to choose a
294 compromised value for P6. Multi-objective optimization is an approach that can
295 provide such a compromised optimal parameter that balances the requirements of many
296 output variables.

297

298 4.2 Multi-objective optimization

299 The results of single-objective optimization from previous section have highlighted
300 the necessity for multi-objective optimization. Many multi-objective optimization
301 methods have been proposed and validated in numerous studies (e.g., [Boyle *et al.*, 2000;
302 Boyle, 2000; Gupta *et al.*, 1998; Yapo *et al.*, 1998; Vrugt *et al.*, 2003; Bastidas *et al.*,
303 1999; Gupta *et al.*, 1999; Leplastrier *et al.*, 2002; Pollacco *et al.*, 2013; Xia *et al.*,
304 2002]), but in the context of this research, we need a method that can satisfy the
305 following constrains: (1) the method should be compatible with surrogate model
306 optimization; (2) for practical reasons, it should provide a single best parameter set
307 instead of a full Pareto optimum set with many non-dominated parameter sets. The
308 Pareto optimal set usually contains hundreds of points, but for large complex dynamic
309 models such as regional or global land surface models, it is generally impractical, and
310 also unnecessary to run the model in an ensemble mode with hundreds of model runs.
311 For regional or global land surface models coupled with atmospheric models, providing
312 only one parameter set that has good simulation ability for most outputs is a more
313 economical and convenient choice.

314 In multi-objective optimization, there have been many methods that can transform
315 multiple objectives to single objective. Among them, the weighting function based
316 method is the most intuitive and widely used one. In this paper, we assign higher
317 weights to the outputs with larger errors. In the research of Liu *et al.* [2005], the RMSE
318 of each outputs were normalized by the RMSE of default parameter set, and each
319 normalized RMSE were assigned equal weights. Van Griensven and Meixner [2007]
320 developed a weighting system based on Bayesian statistics to define ‘high probability
321 regions’ that can give ‘good’ results for multiple outputs. However, both of Liu *et al.*
322 [2005] and van Griensven and Meixner [2007] tended to assign higher weights to the
323 outputs with lower RMSE, and lower weights to the outputs with higher RMSE. This
324 tendency, although reasonable in the probability meaning, conflicts with our intuitive
325 motivations that we want to emphasis on the poorly simulated outputs with large RMSE.
326 Jackson *et al.* [2003] assumed Gaussian error in the data and model so that the outputs

327 were in a joint Gaussian distribution, and the multi-objective ‘cost function’ was
 328 defined on the joint Gaussian distribution of multiple outputs. In *Gupta et al.* [1998], a
 329 multiple weighting function method is proposed to fully describe the Pareto frontier, if
 330 the frontier is convex and model simulation is cheap enough. If one outputs is more
 331 important than others, a higher weight should be assigned to it. *Marler and Arora* [2010]
 332 reviewed the applications, conceptual significance and pitfalls of weighting function
 333 based optimal methods, and gave some suggestions to avoid blind use of it.

334 In this study, we use a weighting function method to convert the multi-objective
 335 optimization into a single objective optimization. The general idea is that we assign
 336 more weight to the objective function of an output, if that output is simulated more
 337 poorly as compared to the other outputs. **Table 4** shows the RMSE and NRMSE of
 338 CoLM using default parameterization scheme, and the weight of each output is
 339 proportional to the NRMSE.

340 [Table 4]

341 After the weights are determined, the weighted objective function is as follows:

$$F = \sum_{i=1}^n w_i RMSE_i \quad (2)$$

342 in which the $RMSE_i$ is the Root Mean Squared Error of each output variable that
 343 defined as $RMSE_i = \frac{1}{N} \sqrt{\sum_{j=1}^N (y_{i,j}^{sim} - y_{i,j}^{obs})^2}$, w_i is the weight of each output, and
 344 $\sum_{i=1}^n w_i = 1$.

345 In order to use the information offered by surrogate model more effectively, we
 346 developed an adaptive surrogate modeling based optimization method called ASMO
 347 [*Wang et al.*, 2014]. The major steps of ASMO are as follows: (1) Construct a surrogate
 348 model with initial samples, and find the optimal parameter of the surrogate model. (2)
 349 Run the original model with this optimal parameter and get a new sample. (3) Add the
 350 new sample to the sample set and construct a new surrogate model, and go back to the
 351 1st step. The effectiveness and efficiency of ASMO have been validated in [*Wang et al.*,
 352 2014] using 6D Hartman function and a simple hydrologic model SAC-SMA. As shown
 353 in the comparison between ASMO and SCE-UA, ASMO is more efficient that can

354 converge with less model runs, while SCE-UA is more effective that can get closer to
355 the true global optimal parameter. So making a choice between ASMO and SCE-UA is
356 a “cost-benefit” trade-off: if the model is very cheap to run, SCE-UA is preferred
357 because it is more effective to find the global optimum; while if the model is very
358 expensive to run, ASMO is preferred because it can find a fairly good parameter within
359 a limited time of model runs. Such parameter set can provide only the approximate
360 global optimum, but this approach is much cheaper than using traditional approaches
361 such as SCE-UA.

362 We carried out multi-objective optimization with ASMO using weighting function
363 defined in **equation (2)** and the optimization results are shown in **figure 4 and 5**. To
364 compare, we also carried out the direct optimization using SCE-UA. **Figure 4** presents
365 the default parameter, the optimal parameter given by ASMO and that given by SCE-
366 UA. **Figure 5** shows the improvements given by ASMO and SCE-UA comparing to the
367 default parameters. From **Figure 5** we can find that all of the outputs are improved
368 nearly 10% except soil temperature, and the improvements made by ASMO is similar
369 to that by SCE-UA. The results indicated that multi-objective optimization can indeed
370 enhance the performance of CoLM using either ASMO or SCE-UA method. The
371 ASMO method get converged after 11 iterations, namely, the total number of model
372 runs is 411, while the number of model runs for SCE-UA is 1000, which is the
373 maximum model runs set for SCE-UA. Obviously ASMO is a more efficient method
374 compared to SCE-UA in this case.

375

376 [Figure 4]

377 [Figure 5]

378

379 We also used the Taylor diagram [*Taylor, 2001*] to compare the simulation results
380 for the calibration period and the validation period (see **figure 6 and 7**). The
381 optimization results given by SCE-UA and ASMO are compared against the
382 performance of default parameterization scheme. Since only 2 years observation data
383 of the 6 output variables are available, we use the first year (2008) data as the warm-up

384 period, use the second year (2009) data as calibration period, and then use the previous
385 2008 year data as the validation period. The missing records have been removed from
386 the comparison.

387 As indicated in **figure 6**, the performance of optimized parameters given by both
388 SCE-UA and ASMO (Case C and D in the Taylor diagram) are better than default
389 parameterization scheme (Case B) except soil temperature. Even though soil
390 temperature simulation is degraded, the correlation coefficients given by all the three
391 cases are higher than 0.9, indicating that this imperfection will not cause significant
392 inconsistency in the land surface modelling. In **figure 7**, the performance of the
393 validation period is shown quite similar to that in the calibration period, indicating that
394 the optimal parameters are well identified and the over-fitting problem is avoided.

395

396 [Figure 6]

397 [Figure 7]

398

399 The four energy fluxes (sensible/latent heat, upward long-wave radiation, net
400 radiation) and soil surface temperature have very good performance. However, the
401 performance of soil moisture seems not satisfactory. The correlation coefficient of soil
402 moisture of Case B(default parameter) is less than 0, while with the help of SCE-UA
403 and ASMO optimization the correlation coefficient is only slightly larger than 0. The
404 possible reasons might be as follows: (1) The default soil parameters of CoLM is
405 derived from the soil texture in the 17-category FAO-STATSGO soil dataset [*Ji and*
406 *Dai, 2010*], which provides top-layer (30cm) and bottom-layer (30-100cm) global soil
407 textures and has a 30 seconds resolution. The resolution and accuracy of this dataset
408 may be not accurate enough in A'rou station, where frequent freezing and thawing occur.
409 A finer soil database, such as 'The Soil Database of China for Land Surface Modeling'
410 [*Shangguan et al., 2013*], or an in-situ field survey for soil texture, should be used to
411 improve the quality of default parameterization scheme; (2) Simulating
412 freezing/thawing processes is a challenging task in land surface modeling, and we are
413 still lack of knowledge about the details of the physical processes. Parameter

414 optimization can improve the model performance if the model physics are correct, but
415 is helpless if the model structure is inconsistent with the true underlying physical
416 processes. Although CoLM's performance of simulating frozen soil and snow cover has
417 been evaluated in the experiment in Valdai, Russia [*Dai et al.*, 2003], the situation of
418 Heihe in China can be very different. For instance, in CoLM the soil depth is set to
419 2.86m globally, but actually the soil depth varies in different places. Fundamentally
420 such a simplification may not introduce significant error to the simulation of energy
421 flux, but it definitely influence the performance of hydrological processes such as soil
422 moisture. Further, the altitude of Heihe is much higher than Valdai, and the influence
423 of human activities is also significantly different. All these reasons can potentially
424 influence the performance of CoLM and cannot be mitigated by parameter optimization.

425 In the optimization results, five of the outputs were improved but only soil
426 temperature became worse. In multi-objective optimization, a compromise is necessary.
427 In this case study, soil temperature requires small P6 and large 36, which conflict with
428 all other outputs. Consequently, improving every output is impossible and some output
429 might be sacrificed. If the cost is affordable and the gain is big enough, such
430 compromise might be worthwhile. In this case study, the smallest weight was assigned
431 to soil temperature. In the optimal solution, the RMSE of soil temperature increases
432 from 2.66 degree to 2.90 degree (only 0.24 degrees larger), but other outputs RMSE
433 can all be improved by about 10%. We think the sacrifice of soil temperature is
434 worthwhile because a negligible degradation of one output can lead to significant
435 improvement of all other outputs.

436 **5. Discussion and Conclusions**

437 We have carried out multi-objective parameter optimization for a land surface
438 model, CoLM, at the Heihe river basin. Although there have been other studies, such
439 as multi-objective calibration of hydrological models [*Gupta et al.*, 1998; *Vrugt et al.*,
440 2003], land surface models [*Gupta et al.*, 1999], single column land-atmosphere
441 coupled model [*Liu et al.*, 2005], and SVAT model [*Pollacco et al.*, 2013], the novel
442 contribution of this research lies in the significant reduction of model runs. In previous
443 researches, a typical multi-objective optimization needs $10^5\sim 10^6$ or even more model

444 runs. For large complex dynamic models which are very expensive to run, parameter
445 optimization is impractical because of lack of computational resources. In this research,
446 we managed to achieve a multi-objective optimal parameter set with only 411 model
447 runs. The performance of the optimal parameter set is similar with the one obtained by
448 SCE-UA method using more than 1000 model runs. Such a result indicates that the
449 proposed framework in this paper is able to provide optimal parameters much efficiently.
450 In the future work, we are going to extend the uncertainty quantification framework to
451 other large complex dynamic models, such as regional-scale land surface models,
452 atmospheric models and climate models. We will look into testing the scalability of the
453 screening, surrogate modelling and optimization techniques on more complex models
454 with more adjustable parameters. We will also investigate the influence of uniformity
455 and stochasticity of initial sampling points, and compare the suitability of different
456 sampling methods. In addition to examining the main and total effects of the parameters,
457 we will also evaluate the interactions among parameters. We will continue to improve
458 the effectiveness, efficiency, flexibility and robustness of Gaussian Processes
459 Regression approach for surrogate modelling, and test with more complex models.
460 Since weighting function based multi-objective optimization methods are simple,
461 intuitive and effective, an inter-comparison of different weighting systems can be an
462 interesting topic worthy of further research. Further, we intend to investigate ways to
463 identify Pareto optimal parameter sets using a surrogate based optimization approach.

464 Discussion and collaborations are warmly welcomed on this and ongoing works.
465 The computer code used in this study is available from the first author, which going to
466 be published as part of the ‘UQlab’ software package in the future.

467

468 **Acknowledgements**

469 This research is supported by Natural Science Foundation of China (Grant
470 No.41075075, No.41375139 and No.51309011), Chinese Ministry of Science and
471 Technology 973 Research Program (No. 2010CB428402) and the Fundamental
472 Research Funds for the Central Universities - Beijing Normal University Research
473 Fund (No.2013YB47). Special thanks are due to “Environmental & Ecological Science

474 Data Center for West China, National Natural Science Foundation of China”
 475 (<http://westdc.westgis.ac.cn>) for providing the meteorological forcing data, to the group
 476 of Prof. Shaomin Liu at State Key Laboratory of Remote Sensing Science, School of
 477 Geography and Remote Sensing Science of Beijing Normal University for providing
 478 the surface flux validation data.

479

480

481 **Appendix A. Surrogate modelling approaches**

482 **A.1 Multivariate Adaptive Regression Splines (MARS)**

483 The Multivariate Adaptive Regression Splines (MARS) model is a kind of flexible
 484 regression model of high dimensional data [*Friedman, 1991*]. It automatically divide
 485 the high-dimensional input space into different partitions with several knots and carry
 486 out linear or nonlinear regression in each partition. It takes the form of an expansion in
 487 product spline basis functions as follows:

$$y = f(\mathbf{x}) = a_0 + \sum_{m=1}^M a_m \prod_{k=1}^{K_m} [s_{km}(x_{v(k,m)} - t_{km})]_+ \quad (\text{A.1})$$

488 where y is the output variable and $\mathbf{x} = (x_1, x_2, \dots, x_n)$ is the n -dimensional input
 489 vector; a_0 is a constant, a_m are weightings of each basis functions, m is the index
 490 of basis functions and M is the total number of basis functions; in each basis function
 491 $B_m(\mathbf{x}) = \prod_{k=1}^{K_m} [s_{km}(x_{v(k,m)} - t_{km})]_+$, k is the index of knots and K_m is the total
 492 number of knots; s_{km} take on value ± 1 and indicate the right/left sense of associated
 493 step function, $v(k, m)$ is the index of the input variable in vector \mathbf{x} , and t_{km}
 494 indicates the knot location of the k -th knot in the m -th basis function.

495 MARS model is built in two stages: the forward pass and the backward pass. The
 496 forward pass builds an over-fitting model includes all input variables, while the
 497 backward pass removes the insensitive input variables one at a time. According to
 498 statistical learning theory, such a build-prune strategy can extract information from
 499 training data and meanwhile avoid the influence of noise [*Hastie et al., 2009*]. Because
 500 of its pruning and fitting ability, MARS method can be used as parameter screening

501 method[Gan et al., 2014; Li et al., 2013; Shahsavani et al., 2010], and also surrogate
 502 modeling method[Razavi et al., 2012; Song et al., 2012; Zhan et al., 2013].

503 **A.2 Gaussian Processes Regression (GPR)**

504 Gaussian Processes Regression (GPR) [Rasmussen and Williams, 2006] is a new
 505 machine learning method based on statistical learning theory and Bayesian theory. It is
 506 suitable for high-dimensional, small-sample nonlinear regression problems. In the
 507 function-space view, a Gaussian process can be completely specified by its mean
 508 function and covariance function:

$$\begin{cases} m(\mathbf{x}) = E[f(\mathbf{x})] \\ k(\mathbf{x}, \mathbf{x}') = E[(f(\mathbf{x}) - m(\mathbf{x}))(f(\mathbf{x}') - m(\mathbf{x}'))] \end{cases} \quad (\text{A.2})$$

509 where $f(\mathbf{x})$ is the Gaussian process with n -dimensional input vector $\mathbf{x} =$
 510 (x_1, x_2, \dots, x_n) , $m(\mathbf{x})$ is its mean function and $k(\mathbf{x}, \mathbf{x}')$ is its covariance function
 511 between two input vectors \mathbf{x} and \mathbf{x}' . For short this Gaussian process can be written as
 512 $f(\mathbf{x}) = GP(m(\mathbf{x}), k(\mathbf{x}, \mathbf{x}'))$.

513 Suppose a nonlinear regression model

$$y = f(\mathbf{x}) + \varepsilon \quad (\text{A.3})$$

514 where \mathbf{x} is the input vector, y is the output variable, and ε is the independent
 515 identically distributed Gaussian noise term with zero mean and variance σ_n^2 . Suppose
 516 \mathbf{y} is the training outputs, X is the training input matrix in which each column is an
 517 input vector, \mathbf{f}_* is the test outputs, X_* is the test input matrix, $K(X, X)$, $K(X, X_*)$
 518 and $K(X_*, X_*)$ denote covariance matrixes of all pairs of training and test inputs. We
 519 can easily write the joint distribution of training and testing inputs and outputs as a joint
 520 Gaussian distribution:

$$\begin{bmatrix} \mathbf{y} \\ \mathbf{f}_* \end{bmatrix} \sim N \left(\mathbf{0}, \begin{bmatrix} K(X, X) + \sigma_n^2 I & K(X, X_*) \\ K(X_*, X) & K(X_*, X_*) \end{bmatrix} \right) \quad (\text{A.4})$$

521 We can derive the mean and variance of predicted outputs from Bayesian theory. The
 522 predictive equations are presented as follows:

$$E(\mathbf{f}_*) = K(X_*, X)[K(X, X) + \sigma_n^2 I]^{-1} \mathbf{y} \quad (\text{A.5})$$

$$\text{cov}(\mathbf{f}_*) = K(X_*, X_*) - K(X_*, X)[K(X, X) + \sigma_n^2 I]^{-1} K(X, X_*) \quad (\text{A.6})$$

523 In this example, the outputs \mathbf{y} is centered to zero so that the mean function is $m(\mathbf{x}) =$
 524 0 , while each element of covariance matrixes equals to the covariance function $k(\mathbf{x}, \mathbf{x}')$

525 of input pairs.

526 The covariance function is the crucial ingredient of Gaussian Processes Regression,
 527 as it encodes the prior knowledge about the input-output relationship. There are many
 528 kinds of covariance functions to choose and users can construct special type of cov-
 529 function depending on their prior knowledge. In this paper, we choose Mart ́en
 530 covariance function:

$$k(r) = \frac{2^{1-\nu}}{\Gamma(\nu)} \left(\frac{\sqrt{2\nu}r}{l} \right)^\nu K_\nu \left(\frac{\sqrt{2\nu}r}{l} \right) \quad (\text{A.7})$$

531 where $r = |\mathbf{x} - \mathbf{x}'|$ is the Euclidian distance between input pair \mathbf{x} and \mathbf{x}' , $K_\nu(\cdot)$ is
 532 a modified Bessel function, ν and l are positive hyper parameters, ν is the shape
 533 factor and l is the scale factor (or characteristic length). The Mart ́en covariance
 534 function is an isotopic cov-function that the covariance only depends on the distance
 535 between \mathbf{x} and \mathbf{x}' . The shape scale ν controls the shape of cov-function: larger ν
 536 leads to a smoother process while small ν leads to a rougher one. If the shape scale
 537 $\nu \rightarrow \infty$ we obtain squared exponential covariance function $k(r) = \exp(-r^2/2l^2)$,
 538 which is also called radial basis function (RBF). The Mart ́en covariance function
 539 becomes a product of a polynomial and an exponential when ν is half-integer: $\nu =$
 540 $p + 1/2$. The most widely used cases are $\nu = 3/2$ and $\nu = 5/2$, as follows:

$$k_{\nu=3/2}(r) = \left(1 + \frac{\sqrt{3}r}{l} \right) \exp \left(-\frac{\sqrt{3}r}{l} \right) \quad (\text{A.8})$$

$$k_{\nu=5/2}(r) = \left(1 + \frac{\sqrt{5}r}{l} + \frac{5r^2}{3l^2} \right) \exp \left(-\frac{\sqrt{5}r}{l} \right) \quad (\text{A.9})$$

541 In this paper, a value of $\nu = 5/2$ was used.

542 To adaptively determine the values of hyper parameters l and σ_n , we use
 543 maximum marginal likelihood method. Because of the properties of Gaussian
 544 distribution, the log-marginal likelihood can be easily obtained as follows:

$$\log[p(\mathbf{y}|X)] = -\frac{1}{2} \mathbf{y}^T (K + \sigma_n^2 I)^{-1} \mathbf{y} - \frac{1}{2} \log|K + \sigma_n^2 I| - \frac{n}{2} \log 2\pi \quad (\text{A.10})$$

545 where $K = K(X, X)$. In the training process of GPR, we used SCE-UA optimization
 546 method [Duan et al., 1993] to find the best l and σ_n .

547 **A.3 Random Forests (RF)**

548 Random Forest (RF) [Breiman, 2001] is a combination of Classification and
 549 Regression Trees (CART) [Breiman *et al.*, 1984]. Generally speaking, Tree-based
 550 methods split the feature space into a set of rectangles and fit the samples in each
 551 rectangle with a class label (for classification problems) or a constant value (for
 552 regression problems). In this paper only regression tree was discussed. Suppose $\mathbf{x} =$
 553 (x_1, x_2, \dots, x_n) is the n -dimensional input feature vector and y is the output response,
 554 the regression tree can be expressed as follows:

$$\hat{f}(\mathbf{x}) = \sum_{m=1}^M c_m I(\mathbf{x} \in R_m) \quad (\text{A.11})$$

$$I(\mathbf{x} \in R_m) = \begin{cases} 1, & \mathbf{x} \in R_m \\ 0, & \mathbf{x} \notin R_m \end{cases} \quad (\text{A.12})$$

555 where M is the total number of rectangles, m is the index of rectangle, R_m is its
 556 corresponding region, c_m is a constant value equals to the mean value of y in region
 557 R_m . To effectively and efficiently find the best binary partition, a greedy algorithm is
 558 used to determine the feature to split and the location of split point. This greedy
 559 algorithm can be very fast especially for large dataset.

560 Because of the major disadvantages of a single tree, such as over-fitting, lack of
 561 smoothness and high variance, many improved methods have been proposed, such as
 562 MARS and random forests. A random forest construct many trees using randomly
 563 selected outputs and features, and synthetic the outputs of all the trees to give the
 564 prediction result. A random forest only have two parameters: the total number of trees
 565 t , and the selected feature number \hat{m} . Constructing random forests needs following
 566 steps:

- 567 1) Bootstrap aggregating (Bagging): From total N samples $(\mathbf{x}_i, y_i), i = 1, 2, \dots, N$,
- 568 randomly select one point at one time with replacement, and replicate N times to
- 569 get a resample set containing N points. This set is called a bootstrap replication. We
- 570 need t bootstrap replications for each tree.
- 571 2) Tree construction: For each splitting of each tree, randomly select \hat{m} features from
- 572 the total M , and select the best fitting feature among the \hat{m} to split. The \hat{m}

573 selected features should be replaced in every splitting step.

574 3) The prediction result of a random forest is given by averaging the output of t trees.

$$\hat{f}_{rf}(\mathbf{x}) = \sum_{j=1}^t \hat{f}_j(\mathbf{x}) \quad (\text{A.13})$$

575 Random forests have outstanding performance for very high dimensional problems,
 576 such as medical diagnosis and document retrieval. Such problems usually have
 577 hundreds or thousands of input variables (features), but each feature provides only a
 578 little information. A single classification or regression model usually has very poor skill
 579 that only slightly better than random prediction. However, by combining many trees
 580 trained with random features, a random forest can give improved accuracy. For big-data
 581 problems that have more than 100 input features and more than one million training
 582 samples, random forests become the only choice because of its outstanding efficiency
 583 and effectiveness.

584 **A.4 Support Vector Machine (SVM)**

585 Support Vector Machine (SVM) is an appealing machine learning method for
 586 classification and regression problems depending on the statistical learning theory
 587 [Vapnik, 1998; 2002]. The SVM method can avoid over-fitting problem because it
 588 employs the structural risk minimization principle. It is also efficient for big-data
 589 because of its scarcity. A brief introduction to support vector regression is presented
 590 below.

591 The aim of SVM is to find a function $f(\mathbf{x})$ that can fit the output y with
 592 minimum risk given a N point training set $(\mathbf{x}_i, y_i), i = 1, 2, \dots, N$. Take a simple linear
 593 regression model for example, the function $f(\mathbf{x})$ can be:

$$f(\mathbf{x}) = \mathbf{w}^T \mathbf{x} + b \quad (\text{A.14})$$

594 where \mathbf{w} is the weighting vector and \mathbf{x} is the n -dimensional input feature vector. This
 595 function is actually determined by a small subset of training samples called support
 596 vectors (SVs).

597 Nonlinear problems can be transferred to linear problems by applying a nonlinear
 598 mapping from low-dimensional input space to some high-dimensional feature space:

$$f(\mathbf{x}) = \mathbf{w}^T \phi(\mathbf{x}) + b \quad (\text{A.15})$$

599 where $\phi(\mathbf{x})$ is the mapping function. The inner product of mapping function is called
 600 Kernel Function: $K(\mathbf{x}, \mathbf{x}') = \phi(\mathbf{x})^T \phi(\mathbf{x}')$ and this method is called Kernel method.
 601 The commonly used kernel functions are: linear kernel function, polynomial, sigmoid
 602 and radial basis function (RBF). In this paper we use RBF kernel:

$$K(\mathbf{x}, \mathbf{x}') = \exp(-\gamma |\mathbf{x} - \mathbf{x}'|^2) \quad (\text{A.16})$$

603 where $|\mathbf{x} - \mathbf{x}'|$ is the Euclidian distance between \mathbf{x} and \mathbf{x}' , γ is a user defined
 604 parameter that controls the smoothness of $f(\mathbf{x})$.

605 To qualify the ‘risk’ of function $f(\mathbf{x})$, a loss function is defined as follows:

$$|y - f(\mathbf{x})|_\varepsilon = \begin{cases} 0, & \text{if } |y - f(\mathbf{x})| \leq \varepsilon \\ |y - f(\mathbf{x})| - \varepsilon, & \text{otherwise} \end{cases} \quad (\text{A.17})$$

606 The loss function means regression errors less than tolerance ε are not penalized. The
 607 penalty-free zone is also called ε -tube or ε -boundary. As explained in statistical
 608 learning theory[Vapnik, 1998], the innovative loss function is the key point that SVM
 609 can balance empirical risk (risk of large error in the training set) and structure risk (risk
 610 of an over-complex model, or over-fitting). The problem of simultaneously minimizing
 611 both empirical risk (represented by regression error) and structure risk (represented by
 612 the width of ε -tube) can be written as a quadratic optimization problem:

$$\begin{aligned} \min_{\mathbf{w}, b, \xi, \xi^*} \quad & \frac{1}{2} \mathbf{w}^T \mathbf{w} + C \sum_{i=1}^n \xi_i + C \sum_{i=1}^n \xi_i^* \\ \text{subject to} \quad & \mathbf{w}^T \phi(\mathbf{x}_i) + b - y_i \leq \varepsilon + \xi_i \\ & y_i - \mathbf{w}^T \phi(\mathbf{x}_i) - b \leq \varepsilon + \xi_i^* \\ & \xi_i, \xi_i^* \geq 0, i = 1, 2, \dots, n \end{aligned} \quad (\text{A.18})$$

613 The problem can be transferred to the dual problem:

$$\begin{aligned} \min_{\mathbf{w}, b, \xi, \xi^*} \quad & \frac{1}{2} (\boldsymbol{\alpha} - \boldsymbol{\alpha}^*)^T \mathbf{K} (\boldsymbol{\alpha} - \boldsymbol{\alpha}^*) + \varepsilon \sum_{i=1}^n (\alpha_i + \alpha_i^*) \\ & + \sum_{i=1}^n y_i (\alpha_i - \alpha_i^*) \\ \text{subject to} \quad & \mathbf{e}^T (\boldsymbol{\alpha} - \boldsymbol{\alpha}^*) = 0 \\ & y_i - \mathbf{w}^T \phi(\mathbf{x}_i) - b \leq \varepsilon + \xi_i^* \\ & 0 \leq \alpha_i, \alpha_i^* \leq C, i = 1, 2, \dots, n \end{aligned} \quad (\text{A.19})$$

614 where \mathbf{K} is the kernel function matrix with $K_{ij} = K(\mathbf{x}_i, \mathbf{x}_j)$. Solving the dual problem

615 and we can get the predictive function:

$$f(\mathbf{x}) = \sum_{i=1}^n (-\alpha_i + \alpha_i^*) K(\mathbf{x}_i, \mathbf{x}) + b \quad (\text{A.20})$$

616 where the vectors $(\boldsymbol{\alpha}^* - \boldsymbol{\alpha})$ are the support vectors (SVs).

617 **A.5 Artificial Neural Network (ANN)**

618 Artificial Neural Network (ANN) [Jain *et al.*, 1996] is time-honored machine
 619 learning method comparing to the former four. It is a data-driven process that can solve
 620 complex nonlinear relationships between input and output data. A neural network is
 621 constructed by many interconnected neurons. Each neuron can be mathematically
 622 described as a linear weighing function and a nonlinear activation function:

$$I_i = \sum_{j=1}^n w_{ij} x_j \quad (\text{A.21})$$

$$f_i(I) = \frac{1}{1 + \exp(-I_i)} \quad (\text{A.22})$$

623 where x_j is the j -th input variable, w_{ij} is the weight and I_i is the weighted sum of
 624 the i -th neuron. The output of the i -th neuron $f_i(I)$ is given by the nonlinear activation
 625 function of the weighted sum input. Here we use Sigmoid function.

626 [Minsky and Papert, 1969] shows that single layer neural network can only solve
 627 linear problem. [Cybenko, 1989] extended ANN to multiple layer and demonstrated that
 628 multi-layer ANN can infinitely approximate any nonlinear function (the universal
 629 approximation theorem). The training procedure of ANN is optimizing the value of
 630 weights. There are many training methods for ANN and we use the Levenberg-
 631 Marquardt (LM) [Marquardt, 1963] algorithm, a modification of the classic Newton
 632 algorithm provided in matlab ANN toolbox.

633

634

635 **References:**

- 636 Bastidas, L. A., H. V. Gupta, S. Sorooshian, W. J. Shuttleworth, and Z. L. Yang (1999), Sensitivity
 637 analysis of a land surface scheme using multicriteria methods, *Journal of Geophysical Research:*
 638 *Atmospheres*, 104(D16), 19481-19490.
- 639 Bonan, G. B. (1996), A Land Surface Model (LSM Version 1.0) for Ecological, Hydrological, and
 640 Atmospheric Studies: Technical Description and User's Guide, NCAR, Boulder, CO, USA.
- 641 Boyle, D. P., H. V. Gupta, and S. Sorooshian (2000), Toward improved calibration of hydrologic models:

- 642 Combining the strengths of manual and automatic methods, *Water Resour Res*, 36(12), 3663-3674.
- 643 Boyle, D. P. (2000), Multicriteria calibration of hydrological models, Ph.D. dissertation thesis,
644 University of Arizona, Tucson, USA.
- 645 Breiman, L., J. Friedman, C. J. Stone, and R. A. Olshen (1984), *Classification and Regression Trees*,
646 Chapman and Hall/CRC, Boca Raton, Florida, USA.
- 647 Breiman, L. (2001), Random forests, *Mach Learn*, 45(1), 5-32.
- 648 Castelletti, A., F. Pianosi, R. Soncini-Sessa, and J. P. Antenucci (2010), A multiobjective response
649 surface approach for improved water quality planning in lakes and reservoirs, *Water Resour Res*, 46(6),
650 W6502.
- 651 Cybenko, G. (1989), Approximation by superpositions of a sigmoidal function, *Mathematics of Control,*
652 *Signals and Systems*, 2(4), 303-314.
- 653 Dai, Y., and Q. Zeng (1997), A Land Surface Model (IAP94) for Climate Studies Part I:Formulation and
654 Validation in Off-Line Experiments, *Adv Atmos Sci*, 14(4), 433-460.
- 655 Dai, Y., F. Xue, and Q. Zeng (1998), A Land Surface Model (IAP94) for Climate Studies Part
656 II:Implementation and Preliminary Results of Coupled Model with IAP GCM, *Adv Atmos Sci*, 15(4), 47-
657 62.
- 658 Dai, Y. J., X. B. Zeng, R. E. Dickinson, I. Baker, G. B. Bonan, M. G. Bosilovich, A. S. Denning, P. A.
659 Dirmeyer, P. R. Houser, G. Y. Niu, K. W. Oleson, C. A. Schlosser, and Z. L. Yang (2003), The Common
660 Land Model, *B Am Meteorol Soc*, 84(8), 1013-1023.
- 661 Dai, Y. J., R. E. Dickinson, and Y. P. Wang (2004), A two-big-leaf model for canopy temperature,
662 photosynthesis, and stomatal conductance, *J Climate*, 17(12), 2281-2299.
- 663 Dickinson, R. E., A. Henderson-Sellers, and P. J. Kennedy (1993), Biosphere-atmosphere Transfer
664 Scheme (BATS) Version 1e as Coupled to the NCAR Community Climate Model, NCAR, Boulder, CO.
665 USA.
- 666 Duan, Q. Y., S. Sorooshian, and V. K. Gupta (1992), Effective and Efficient Global Optimization for
667 Conceptual Rainfall-Runoff Models, *Water Resour Res*, 28(4), 1015-1031.
- 668 Duan, Q. Y., V. K. Gupta, and S. Sorooshian (1993), Shuffled Complex Evolution Approach for
669 Effective and Efficient Global Minimization, *J Optimiz Theory App*, 76(3), 501-521.
- 670 Duan, Q. Y., S. Sorooshian, and V. K. Gupta (1994), Optimal Use of the SCE-UA Global Optimization
671 Method for Calibrating Watershed Models, *J Hydrol*, 158(3-4), 265-284.
- 672 Friedman, J. H. (1991), Multivariate Adaptive Regression Splines, *Ann Stat*, 19(1), 1-14.
- 673 Gan, Y., Q. Duan, W. Gong, C. Tong, Y. Sun, W. Chu, A. Ye, C. Miao, and Z. Di (2014), A
674 comprehensive evaluation of various sensitivity analysis methods: A case study with a hydrological
675 model, *Environ Modell Softw*, 51(0), 269-285.
- 676 Gorissen, D. (2010), Grid-enabled Adaptive Surrogate Modeling for Computer Aided Engineering, Ph.D.
677 thesis, Ghent University, Ghent, Flanders, Belgium.
- 678 Gupta, H. V., S. Sorooshian, and P. O. Yapo (1998), Toward improved calibration of hydrologic models:
679 Multiple and noncommensurable measures of information, *Water Resour Res*, 34(4), 751-763.
- 680 Gupta, H. V., L. A. Bastidas, S. Sorooshian, W. J. Shuttleworth, and Z. L. Yang (1999), Parameter
681 estimation of a land surface scheme using multicriteria methods, *J Geophys Res*, 104(D16), 19491-19503.
- 682 Hastie, T., R. Tibshirani, and J. Friedman (2009), *The Elements of Statistical Learning 2nd*, Springer,
683 New York, USA.
- 684 Henderson-Sellers, A., K. McGuffie, and A. J. Pitman (1996), The Project for Intercomparison of Land-
685 surface Parametrization Schemes (PILPS): 1992 to 1995, *Clim Dynam*, 12(12), 849-859.

- 686 Hu, Z. Y., M. G. Ma, R. Jin, W. Z. Wang, G. H. Huang, Z. H. Zhang, and J. L. Tan (2003), WATER:
 687 dataset of automatic meteorological observations at the A'rou freeze/thaw observation station, Cold and
 688 Arid Regions Environmental and Engineering Research Institute, Chinese Academy of Sciences,
 689 Lanzhou, China.
- 690 Jackson, C., Y. Xia, M. K. Sen, and P. L. Stoffa (2003), Optimal parameter and uncertainty estimation
 691 of a land surface model: A case study using data from Cabauw, Netherlands, *Journal of Geophysical*
 692 *Research: Atmospheres*, 108(D18), 4583.
- 693 Jain, A. K., M. Jianchang, and K. M. Mohiuddin (1996), Artificial neural networks: a tutorial, *Computer*,
 694 29(3), 31-44.
- 695 Ji, D., and Y. Dai (2010), The Common Land Model (CoLM) technical guide, GCESS, Beijing Normal
 696 University, Beijing, China.
- 697 Jin, Y. (2011), Surrogate-assisted evolutionary computation: Recent advances and future challenges,
 698 *Swarm and Evolutionary Computation*, 1(2), 61-70.
- 699 Jones, D. R., M. Schonlau, and W. J. Welch (1998), Efficient global optimization of expensive black-
 700 box functions, *J Global Optim*, 13(4), 455-492.
- 701 Jones, D. R. (2001), A Taxonomy of Global Optimization Methods Based on Response Surfaces, *J*
 702 *Global Optim*, 21(4), 345-383.
- 703 Koziel, S., and L. Leifsson (2013), *Surrogate-Based Modeling and Optimization*, Springer New York,
 704 New York, NY.
- 705 Leplastrier, M., A. J. Pitman, H. Gupta, and Y. Xia (2002), Exploring the relationship between
 706 complexity and performance in a land surface model using the multicriteria method, *J Geophys Res*,
 707 107(4443D20).
- 708 Li, J. (2012), Screening and Analysis of Parameters Most Sensitive to CoLM, Master thesis, BNU,
 709 Beijing, China.
- 710 Li, J., Q. Y. Duan, W. Gong, A. Ye, Y. Dai, C. Miao, Z. Di, C. Tong, and Y. Sun (2013), Assessing
 711 parameter importance of the Common Land Model based on qualitative and quantitative sensitivity
 712 analysis, *Hydrol. Earth Syst. Sci.*, 17(8), 3279-3293.
- 713 Liang, X., E. F. Wood, D. P. Lettenmaier, D. Lohmann, A. Boone, S. Chang, F. Chen, Y. Dai, C.
 714 Desborough, R. E. Dickinson, Q. Duan, M. Ek, Y. M. Gusev, F. Habets, P. Irannejad, R. Koster, K. E.
 715 Mitchell, O. N. Nasonova, J. Noilhan, J. Schaake, A. Schlosser, Y. Shao, A. B. Shmakin, D. Verseghy,
 716 K. Warrach, P. Wetzel, Y. Xue, Z. Yang, and Q. Zeng (1998), The Project for Intercomparison of Land-
 717 surface Parameterization Schemes (PILPS) phase 2(c) Red-Arkansas River basin experiment:: 2. Spatial
 718 and temporal analysis of energy fluxes, *Global Planet Change*, 19(1 - 4), 137-159.
- 719 Liu, Y. Q., L. A. Bastidas, H. V. Gupta, and S. Sorooshian (2003), Impacts of a parameterization
 720 deficiency on offline and coupled land surface model simulations, *J Hydrometeorol*, 4(5), 901-914.
- 721 Liu, Y. Q., H. V. Gupta, S. Sorooshian, L. A. Bastidas, and W. J. Shuttleworth (2004), Exploring
 722 parameter sensitivities of the land surface using a locally coupled land-atmosphere model, *J Geophys*
 723 *Res*, 109(D21101D21), 13.
- 724 Liu, Y. Q., H. V. Gupta, S. Sorooshian, L. A. Bastidas, and W. J. Shuttleworth (2005), Constraining land
 725 surface and atmospheric parameters of a locally coupled model using observational data, *J*
 726 *Hydrometeorol*, 6(2), 156-172.
- 727 Lohmann, D., D. P. Lettenmaier, X. Liang, E. F. Wood, A. Boone, S. Chang, F. Chen, Y. Dai, C.
 728 Desborough, R. E. Dickinson, Q. Duan, M. Ek, Y. M. Gusev, F. Habets, P. Irannejad, R. Koster, K. E.
 729 Mitchell, O. N. Nasonova, J. Noilhan, J. Schaake, A. Schlosser, Y. Shao, A. B. Shmakin, D. Verseghy,

- 730 K. Warrach, P. Wetzel, Y. Xue, Z. Yang, and Q. Zeng (1998), The Project for Intercomparison of Land-
 731 surface Parameterization Schemes (PILPS) phase 2(c) Red - Arkansas River basin experiment:: 3.
 732 Spatial and temporal analysis of water fluxes, *Global Planet Change*, 19(1 - 4), 161-179.
- 733 Loshchilov, I., M. Schoenauer, and M. E. L. Sebag (2010), Comparison-based Optimizers Need
 734 Comparison-based Surrogates, in Proceedings of the 11th International Conference on Parallel Problem
 735 Solving from Nature: Part I, pp. 364-373, Berlin, Heidelberg.
- 736 Marler, R. T., and J. Arora (2010), The weighted sum method for multi-objective optimization: new
 737 insights, *Struct Multidiscip O*, 41(6), 853-862.
- 738 Marquardt, D. W. (1963), An Algorithm for Least-Squares Estimation of Nonlinear Parameters, *Journal*
 739 *of the Society for Industrial and Applied Mathematics*, 11(2), 431-441.
- 740 McKay, M. D., R. J. Beckman, and W. J. Conover (1979), A Comparison of Three Methods for Selecting
 741 Values of Input Variables in the Analysis of Output from a Computer Code, *Technometrics*, 21(2), 239-
 742 245.
- 743 Minsky, M., and S. A. Papert (1969), *Perceptrons: An Introduction to Computational Geometry*, MIT
 744 Press, Cambridge, Massachusetts, USA.
- 745 Ong, Y., P. B. Nair, A. J. Keane, and K. W. Wong (2005), Surrogate-Assisted Evolutionary Optimization
 746 Frameworks for High-Fidelity Engineering Design Problems, In ‘Studies in Fuzziness and Soft
 747 Computing’, edited by Y. Jin, pp. 307-331, Springer Berlin Heidelberg.
- 748 Pil á, M., and R. Neruda (2013), Surrogate model selection for evolutionary multiobjective optimization,
 749 paper presented at Evolutionary Computation (CEC), 2013 IEEE Congress on, 2013-01-01.
- 750 Pollacco, J. A. P., B. P. Mohanty, and A. Efstratiadis (2013), Weighted objective function selector
 751 algorithm for parameter estimation of SVAT models with remote sensing data, *Water Resour Res*, 49(10),
 752 6959-6978.
- 753 Rasmussen, C. E., and C. K. I. Williams (2006), *Gaussian Processes for Machine Learning*, MIT Press,
 754 Massachusetts, USA.
- 755 Razavi, S., B. A. Tolson, and D. H. Burn (2012), Review of surrogate modeling in water resources, *Water*
 756 *Resour Res*, 48(7), W7401.
- 757 Shahsavani, D., S. Tarantola, and M. Ratto (2010), Evaluation of MARS modeling technique for
 758 sensitivity analysis of model output, *Procedia - Social and Behavioral Sciences*, 2(6), 7737-7738.
- 759 Shangguan, W., Y. Dai, B. Liu, A. Zhu, Q. Duan, L. Wu, D. Ji, A. Ye, H. Yuan, Q. Zhang, D. Chen, M.
 760 Chen, J. Chu, Y. Dou, J. Guo, H. Li, J. Li, L. Liang, X. Liang, H. Liu, S. Liu, C. Miao, and Y. Zhang
 761 (2013), A China data set of soil properties for land surface modeling, *Journal of Advances in Modeling*
 762 *Earth Systems*, 5(2), 212-224.
- 763 Song, X., C. Zhan, and J. Xia (2012), Integration of a statistical emulator approach with the SCE-UA
 764 method for parameter optimization of a hydrological model, *Chinese Sci Bull*, 57(26), 3397-3403.
- 765 Taylor, K. E. (2001), Summarizing multiple aspects of model performance in a single diagram, *Journal*
 766 *of Geophysical Research: Atmospheres*, 106(D7), 7183-7192.
- 767 van Griensven, A., and T. Meixner (2007), A global and efficient multi-objective auto-calibration and
 768 uncertainty estimation method for water quality catchment models, *JOURNAL OF*
 769 *HYDROINFORMATICS*, 9(4), 277-291.
- 770 Vapnik, V. N. (1998), *Statistical Learning Theory*, John Wiley & Sons, NewYork, USA.
- 771 Vapnik, V. N. (2002), *The Nature of Statistical Learning Theory*, 2nd ed., Springer, New York.
- 772 Vrugt, J. A., H. V. Gupta, W. Bouten, and S. Sorooshian (2003), A Shuffled Complex Evolution
 773 Metropolis algorithm for optimization and uncertainty assessment of hydrologic model parameters,

774 *Water Resour Res*, 39(12018), 1201.

775 Vrugt, J. A., H. V. Gupta, L. A. Bastidas, W. Bouten, and S. Sorooshian (2003), Effective and efficient
776 algorithm for multiobjective optimization of hydrologic models, *Water Resour Res*, 39(12148), 1214.

777 Wang, C., Q. Duan, W. Gong, A. Ye, Z. Di, and C. Miao (2014), An evaluation of adaptive surrogate
778 modeling based optimization with two benchmark problems, *Environ Modell Softw*, 60(0), 167-179.

779 Wang, Q. J. (1991), The Genetic Algorithm and Its Application to Calibrating Conceptual Rainfall-
780 Runoff Models, *Water Resour Res*, 27(9), 2467-2471.

781 Wood, E. F., D. P. Lettenmaier, X. Liang, D. Lohmann, A. Boone, S. Chang, F. Chen, Y. Dai, R. E.
782 Dickinson, Q. Duan, M. Ek, Y. M. Gusev, F. Habets, P. Irannejad, R. Koster, K. E. Mitchel, O. N.
783 Nasonova, J. Noilhan, J. Schaake, A. Schlosser, Y. Shao, A. B. Shmakin, D. Verseghy, K. Warrach, P.
784 Wetzel, Y. Xue, Z. Yang, and Q. Zeng (1998), The Project for Intercomparison of Land-surface
785 Parameterization Schemes (PILPS) Phase 2(c) Red - Arkansas River basin experiment:: 1. Experiment
786 description and summary intercomparisons, *Global Planet Change*, 19(1 - 4), 115-135.

787 Xia, Y., A. J. Pittman, H. V. Gupta, M. Leplastrier, A. Henderson-Sellers, and L. A. Bastidas (2002),
788 Calibrating a land surface model of varying complexity using multicriteria methods and the Cabauw
789 dataset, *J Hydrometeorol*, 3(2), 181-194.

790 Yapo, P. O., H. V. Gupta, and S. Sorooshian (1998), Multi-objective global optimization for hydrologic
791 models, *J Hydrol*, 204(1-4), 83-97.

792 Zhan, C., X. Song, J. Xia, and C. Tong (2013), An efficient integrated approach for global sensitivity
793 analysis of hydrological model parameters, *Environ Modell Softw*, 41(0), 39-52.

794

795

796

797 **Figure list:**

798 **Figure 1:** Inter-comparison of 5 surrogate modelling methods, error of training set.

799 **Figure 2:** Inter-comparison of 5 surrogate modelling methods, error of testing set.

800 **Figure 3:** Single-objective optimization result: optimal parameters.

801 **Figure 4:** Optimal value of CoLM given by multi-objective optimization (comparing default
802 parameter, optimal parameter given by ASMO and SCE-UA)

803 **Figure 5:** Comparing the improvements given by ASMO and SCE.

804 **Figure 6:** Taylor diagram of simulated fluxes during calibration period (Jan-1-2009 to Dec-31-
805 2009).

806 **Figure 7:** Taylor diagram of simulated fluxes during validation period (Here we use warm-up period
807 as validation period, Jan-1-2008 to Dec-31-2008).

808

809

810

811

Table 1: Adjustable parameters and their categories, meanings and ranges.

Num	Para	Units	Category	Physical meaning	Feasible range
P1	dewmx		canopy	maximum dew ponding of leaf area	[0.05, 0.15]
P2	hksati	mm/s	soil	maximum hydraulic conductivity	[0.001, 1]
P3	porsl	-	soil	porosity	[0.25, 0.75]
P4	phi0	mm	soil	minimum soil suction	[50, 500]
P5	wtfact		soil	fraction of shallow groundwater area	[0.15, 0.45]
P6	bsw	--	soil	Clapp and Hornberger "b" parameter	[2.5, 7.5]
P7	wimp		soil	water impermeable if porosity less than wimp	[0.01, 0.1]
P8	zInd	m	soil	roughness length for soil surface	[0.005, 0.015]
P9	pondmx	mm	soil	maximum ponding depth for soil surface	[5, 15]
P10	csoilc	--	soil	drag coefficient for soil under canopy	[0.002, 0.006]
P11	zsno	m	snow	roughness length for snow	[0.0012, 0.0036]
P12	capr		soil	tuning factor of soil surface temperature	[0.17, 0.51]
P13	cnfac		canopy	Crank Nicholson factor	[0.25, 0.5]
P14	shti		canopy	slope of low temperature inhibition function	[0.1, 0.3]
P15	hhti		canopy	1/2 point of low temperature inhibition function	[278, 288]
P16	shti		canopy	slope of high temperature inhibition function	[0.15, 0.45]
P17	sqrtdi	m ^{-0.5}	canopy	the inverse of square root of leaf dimension	[2.5, 7.5]
P18	effcon	mol CO ² / mol quanta	canopy	quantum efficiency of vegetation photosynthesis	[0.035, 0.35]
P19	vmax25	mol CO ² / m ² s	canopy	maximum carboxylation rate at 25°C	[10 ⁻⁶ , 200 ⁻⁶]
P20	hhti		canopy	1/2 point of high temperature inhibition function	[305, 315]
P21	trda		canopy	temperature coefficient of conductance-photosynthesis model	[0.65, 1.95]
P22	trdm		canopy	temperature coefficient of conductance-photosynthesis model	[300, 350]
P23	trop		canopy	temperature coefficient of conductance-photosynthesis model	[250, 300]
P24	gradm		canopy	slope of conductance-photosynthesis model	[4, 9]
P25	binter		canopy	intercept of conductance-photosynthesis model	[0.01, 0.04]
P26	extkn		canopy	coefficient of leaf nitrogen allocation	[0.5, 0.75]
P27	chil		canopy	leaf angle distribution factor	[-0.3, 0.1]
P28	ref(1,1)		canopy	VIS reflectance of living leaf	[0.07, 0.105]
P29	ref(1,2)		canopy	VIS reflectance of dead leaf	[0.16, 0.36]
P30	ref(2,1)		canopy	NIR reflectance of living leaf	[0.35, 0.58]
P31	ref(2,2)		canopy	NIR reflectance of dead leaf	[0.39, 0.58]
P32	tran(1,1)		canopy	VIS transmittance of living leaf	[0.04, 0.08]
P33	tran(1,2)		canopy	VIS transmittance of dead leaf	[0.1, 0.3]
P34	tran(2,1)		canopy	NIR transmittance of living leaf	[0.1, 0.3]

Surrogate based parameter optimization of CoLM

P35	tran(2,2)		canopy	NIR transmittance of dead leaf	[0.3, 0.5]
P36	z0m	m	canopy	aerodynamic roughness length	[0.05, 0.3]
P37	ssi		snow	irreducible water saturation of snow	[0.03, 0.04]
P38	smpmax	mm	soil	wilting point potential	[-2.e5, -1.e5]
P39	smpmin	mm	soil	restriction for min of soil potential	[-1.e8, -9.e7]
P40	trsmx0	mm/s	canopy	maximum transpiration for vegetation	[1.e-4, 1. e-2]

813

814

815

Table 2: Screened parameters of CoLM in A'rou Station [Li et.al., 2013]

Output variables (fluxes)	Screened parameters
Sensible Heat	P2, P4, P6, P30, P34, P36
Latent Heat	P3, P4, P6, P18, P19, P23, P25, P36
Upward Longwave Radiation	P6, P17, P36
Net radiation	P6, P17, P30, P34, P36
Soil Temperature	P3, P6, P36
Soil Moisture	P3, P6

816

817

818

819 **Table 3:** The NRMSE between simulated and observed outputs after single objective optimization

	Sensible heat	Latent heat	Upward longwave radiation	Net radiation	Soil Temperature	Soil Moisture
Default	0.8586	0.5833	0.0590	0.2357	0.0096	0.4527
SCE	0.7450	0.4921	0.0380	0.1963	0.0073	0.3900
Optimized	(1492)	(1354)	(458)	(982)	(473)	(210)
LH50	0.7672	0.5255	0.0377	0.1913	0.0080	0.4222
LH100	0.7841	0.5785	0.0372	0.1908	0.0077	0.4130
LH200	0.7821	0.5885	0.0374	0.1928	0.0069	0.3947
LH400	0.7798	0.5627	0.0374	0.1928	0.0070	0.3971
LH800	0.7683	0.5024	0.0377	0.1909	0.0068	0.3956
LH1200	0.7760	0.5150	0.0374	0.1919	0.0068	0.3962
LH2000	0.7705	0.5048	0.0375	0.1912	0.0070	0.3946

820

821

822

823

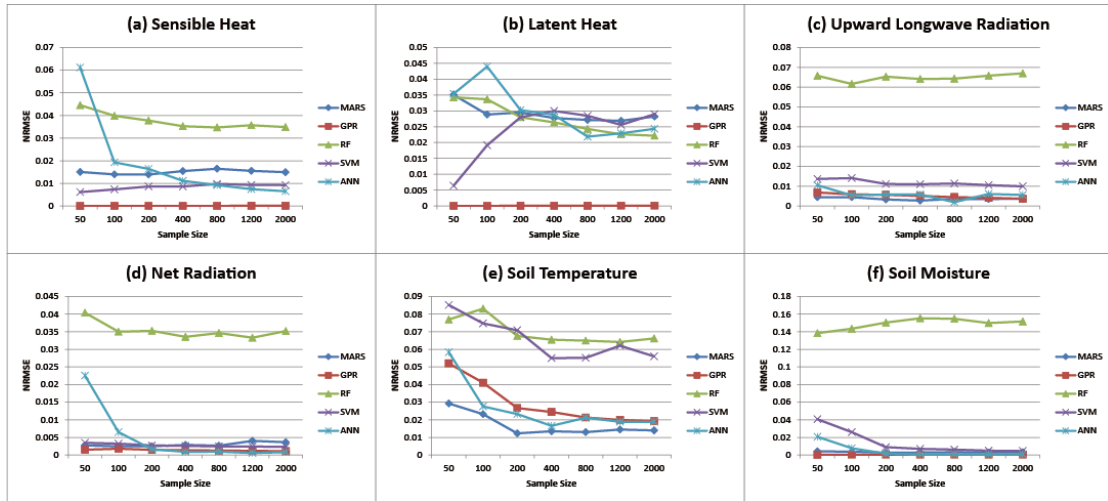
Table 4: Weights assigned to each output variables.

Flux name	Label	Unit	RMSE	NRMSE	Weights
Sensible heat	fsena	W/m ²	49.14	0.8586	0.3905
Latent heat	lfevpa	W/m ²	43.59	0.5833	0.2653
Upward longwave radiation	orlg	W/m ²	19.43	0.0590	0.0268
Net radiation	sabvg	W/m ²	42.78	0.2357	0.1072
Soil temperature	tss	K	2.66	0.0096	0.0044
Soil moisture	wliq	kg/m ²	21.14	0.4527	0.2059

824

825

Surrogate based parameter optimization of CoLM



826

827

Figure 1: Inter-comparison of 5 surrogate modelling methods, error of training set.

828

Surrogate based parameter optimization of CoLM

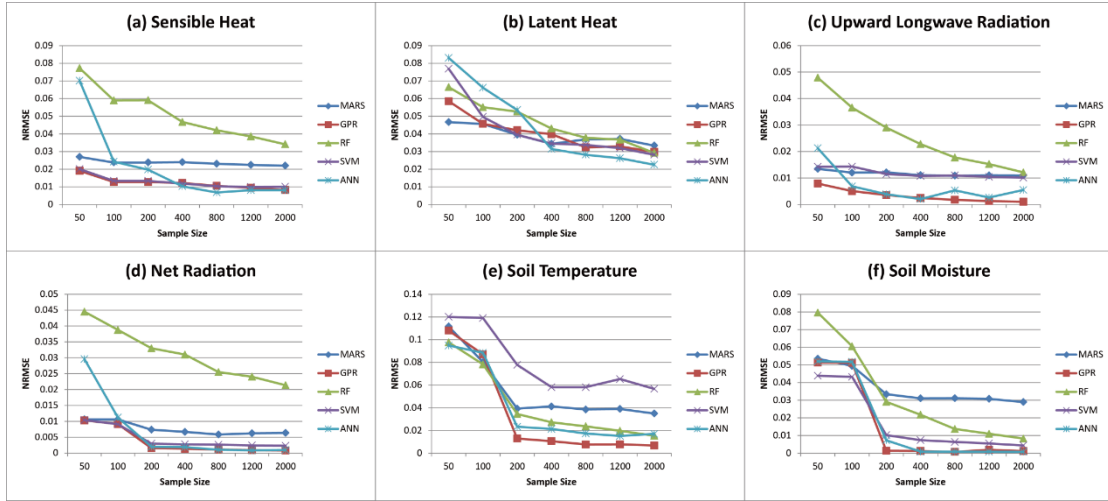


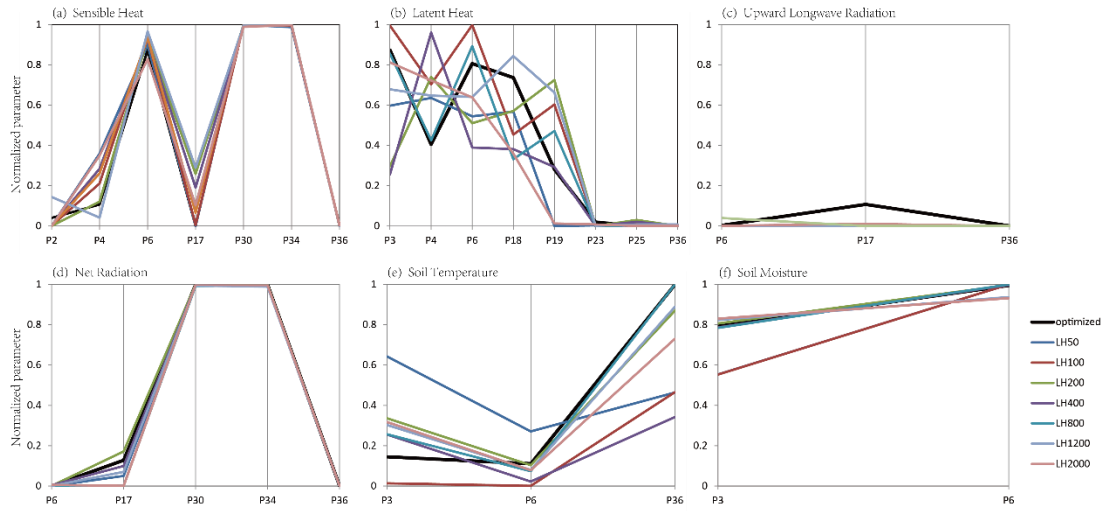
Figure 2: Inter-comparison of 5 surrogate modelling methods, error of testing set.

829

830

831

Surrogate based parameter optimization of CoLM



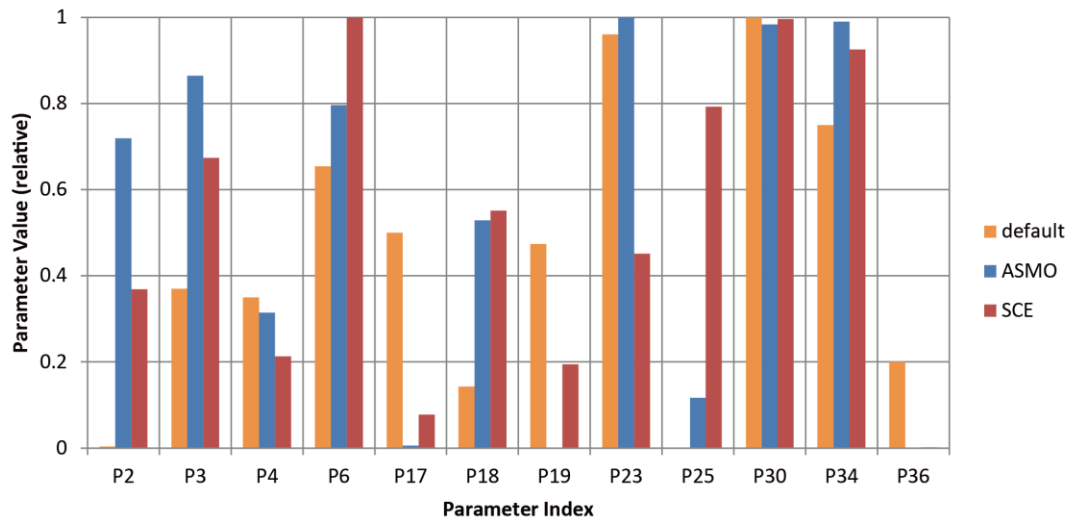
832

833

Figure 2: Single-objective optimization result: optimal parameters.

834

Surrogate based parameter optimization of CoLM



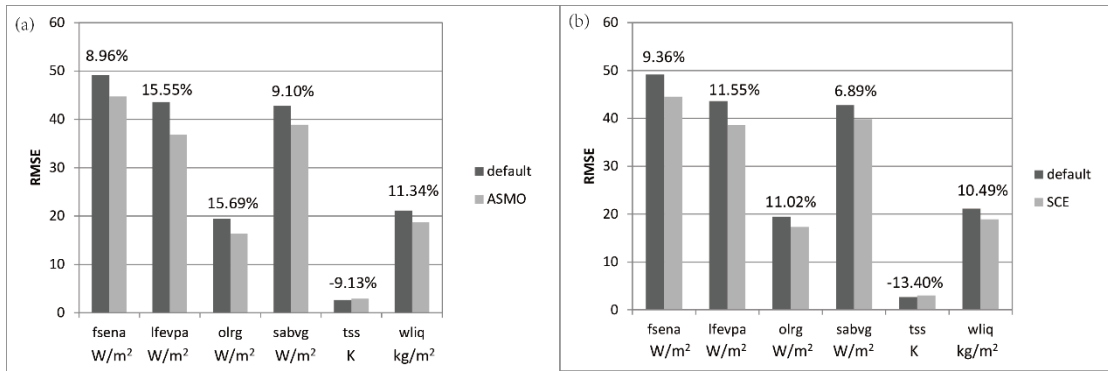
835

836 **Figure 3:** Optimal value of CoLM given by multi-objective optimization (comparing default
837 parameter, optimal parameter given by ASMO and SCE-UA)

838

Surrogate based parameter optimization of CoLM

839



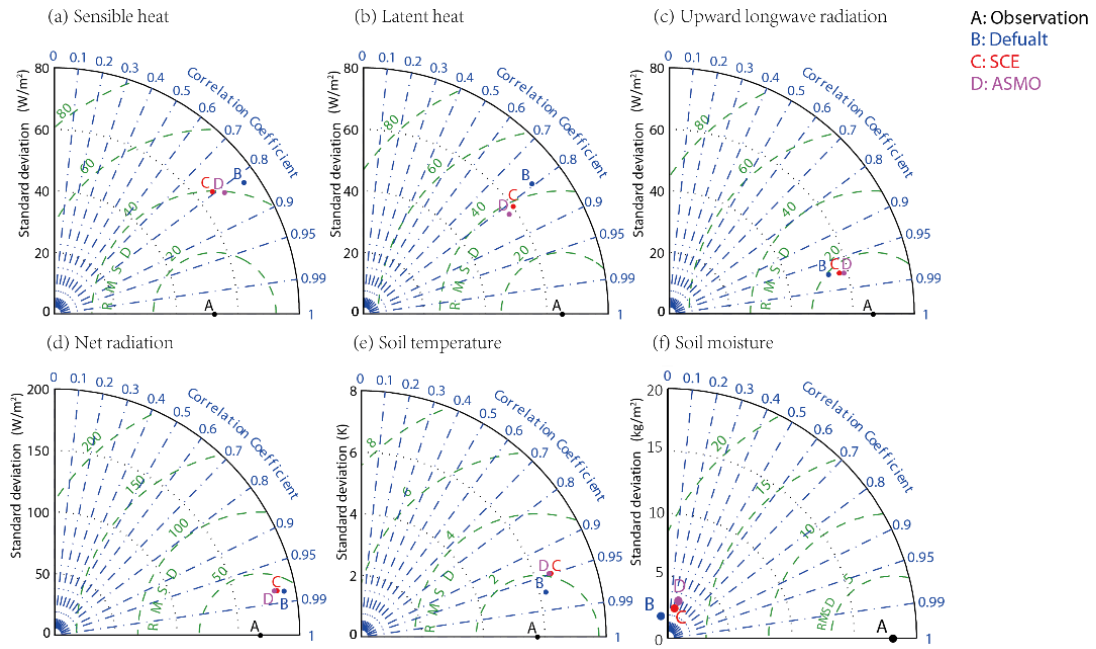
840

841

Figure 4: Comparing the improvements given by ASMO and SCE.

842

Surrogate based parameter optimization of CoLM



843

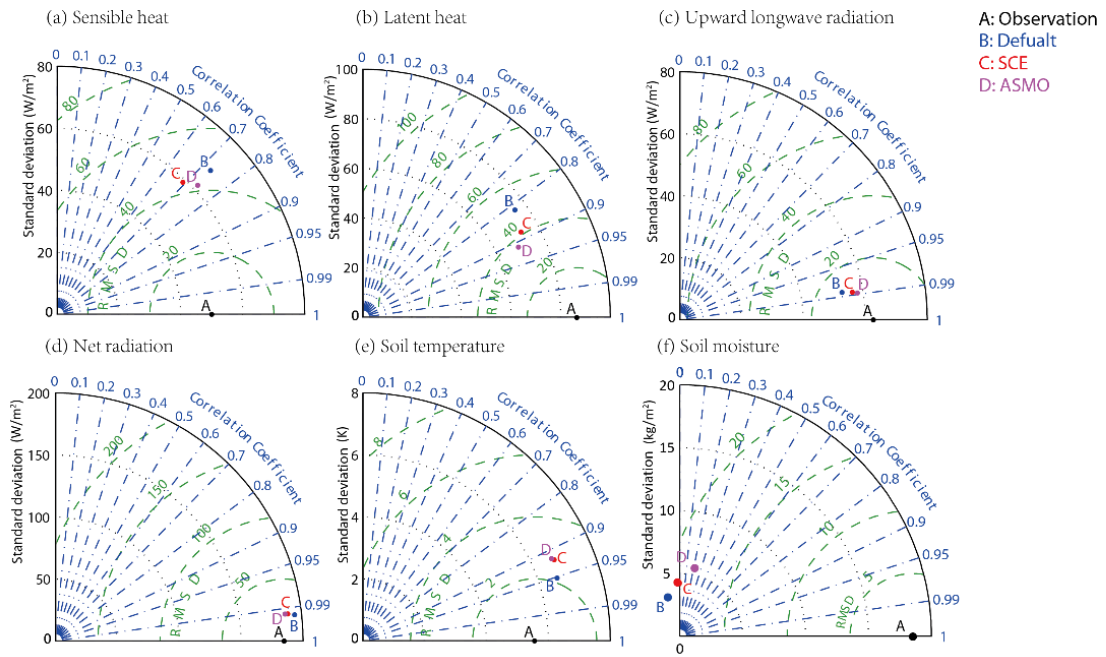
844 **Figure 5:** Taylor diagram of simulated fluxes during calibration period (Jan-1-2009 to Dec-31-

845

2009).

846

847



848

849 **Figure 6:** Taylor diagram of simulated fluxes during validation period (Here we use warm-up

850

period as validation period, Jan-1-2008 to Dec-31-2008).

851

852